

New strategies for submicron characterization the carbon binding of reactive minerals in long-term contrasting fertilized soils: Implications for soil carbon storage

Jian Xiao¹, Xinhua He², Ying Zhou³, Lirong Zheng⁴, Jialong Hao⁵, Wei Ran¹, Qirong Shen¹, Guanghui Yu^{1,6*}

5 ¹ National Engineering Research Center for Organic-based Fertilizers, Jiangsu Collaborative Innovation Center for Solid Organic Waste Resource Utilization, Jiangsu Provincial Key Lab for Organic Solid Waste Utilization, Nanjing Agricultural University, Nanjing 210095, China

² School of Plant Biology, University of Western Australia, Crawley, WA 6009, Australia

³ Shanghai Institute of Measurement and Testing Technology, Shanghai 201203, China

10 ⁴ Beijing Synchrotron Radiation Facility, Institute of High Energy Physics, Chinese Academy of Sciences, Beijing 100049, China

⁵ Key Laboratory of Earth and Planetary Physics, Institute of Geology and Geophysics, Chinese Academy of Science, Beijing 100029, China

⁶ Department of Plant Pathology, North Carolina State University, Raleigh, NC 27695, USA.

15 * *Correspondence to:* G. H. Yu (yuguanghui@njau.edu.cn or gyu6@ncsu.edu)

Abstract. Mineral binding is a major mechanism for soil carbon (C) stabilization. However, the submicron information about the *in situ* mechanisms of different fertilization practices affecting organo-mineral complexes and associated C preservation remains unclear. Here, we applied nano-scale secondary ion mass spectrometry (NanoSIMS), X-ray photoelectron spectroscopy (XPS), and X-ray absorption fine structure spectroscopy (XAFS) to examine differentiating effects of inorganic versus organic fertilization on interactions between highly reactive minerals and soil C preservation. To examine such interactions, soils and their extracted colloids were collected during a 24-year long-term fertilization period (1990-2014) (no-fertilization, Control; chemical nitrogen (N), phosphorus (P) and potassium (K) fertilization, NPK; and NPK plus swine manure fertilization, NPKM). The results for different fertilization conditions showed a ranked soil organic matter (SOM) concentration with NPKM > NPK > Control. Meanwhile, oxalate extracted Al (Al_o), Fe (Fe_o), short range ordered (SRO) Al (Al_{xps}), Fe (Fe_{xps}), and dissolved organic carbon (DOC) ranked with NPKM > Control > NPK, but ratios of DOC/Al_{xps} and DOC/Fe_{xps} ranked with NPKM > NPK > Control. Compared with the NPK treatment, NPKM treatment enhanced the C binding loadings of Al and Fe minerals in soil colloids at the submicron scale. Furthermore, a greater concentration of highly reactive Al and Fe minerals was present under NPKM than under NPK. Together, these submicron scale findings suggest that both reactive mineral species and their associations with C are differentially affected by inorganic and organic fertilization.

Key words: Al and Fe minerals; inorganic and organic fertilization; organo-mineral complexes; reactive minerals; carbon binding capability; X-ray photoelectron spectroscopy (XPS)

1. Introduction

Associations of organic matter (OM) with pedogenic minerals, which are termed as organo-mineral complexes, are known to be key controls in the biogeochemical processes that retain OM in natural soil system (Torn et al., 1997; Kögel-knbaner et al., 2008; Mikutta et al., 2009; Schmidt et al., 2011). Soil OM (SOM) preferentially binds to rough surfaces, which provide a multitude of reactive mineral surfaces (Chen et al., 2014; Vogel et al., 2014). These reactive minerals are also termed as short-range ordered (SRO) meta-stable colloidal minerals in volcanic ejecta (Torn et al., 1997), and serve as the nuclei for soil organic carbon (SOC) storage (Hochella et al., 2008; Kögel-Knabner et al., 2008; Remusat et al., 2012; Vogel et al., 2014). Therefore, reactive Al and Fe minerals in soil play a critical role in determining C stability (Solomon et al., 2012; Hernes et al., 2013).

On the other hand, the reactive mineral surface of organo-mineral complexes in the complex soil matrix (mainly the top-soil layer) could be greatly improved through organic amendments to soil, such as the anthropogenic importation of organic fertilizers under long-term experimentation (Schmidt et al., 2011; Hernandez et al., 2012; Yu et al., 2012; Wen et al., 2014a; Abdala et al., 2015). Based on a meta-analysis of 49 sites and 130 observations in the world, Maillard and Angers (2014) found that cumulative manure input had a dominant effect on SOC stock changes when compared to no fertilization and chemical fertilization (Maillard and Angers, 2014). Furthermore, it was estimated that cumulative manure-C input resulted in a relative SOC change factor of 1.26 ± 0.14 (95% CI). Another meta-analysis assessed and identified the effects of improved farming practices on SOC sequestration in China by compiling a data set of 83 studies (Zhao et al., 2015), indicating that SOC concentration and

stocks at 0-30 cm depth significantly increased when compared to no fertilization and chemical fertilization. Although our previous results had shown that manure amendments enhanced reactive components of minerals (i.e., ferrihydrite and allophane) in soils by selective extraction methods, spectroscopies and high resolution-transmission electron microscopy (HRTEM) observation (Yu et al., 2012; Wen et al., 2014a and 2014b; Huang et al., 2016), little is known about the impacts of different fertilization practices on the *in situ* associations between reactive minerals and SOC in soil colloids at submicron scale.

In general, *in situ* investigations of natural organo-mineral complexes are restricted to bulk analyses of operationally defined physical fractions (Hatton et al., 2012 and 2015; Remusat et al., 2012; Vogel et al., 2014). In contrast, techniques for direct visualization at the submicron scale could greatly aid in gaining a better understanding of the interactions between organic structures and reactive minerals (Remusat et al., 2012; Vogel et al., 2014; Xiao et al., 2015). For instance, nano-scale secondary ion mass spectrometry (NanoSIMS) has the potential to examine the spatial integrity of soil microenvironments and has been designed for high lateral resolution (down to 50 nm) imaging, while still maintaining high mass resolution and high sensitivity (mg kg^{-1} range) (Herrmann et al., 2007; Xiao et al., 2015). Previous studies have shown that NanoSIMS is an effective technique for studying natural organo-mineral complexes at the submicron scale (Herrmann, 2007; Mueller et al., 2012; Remusat et al., 2012; Hatton et al., 2012 and 2015; Vogel et al., 2014). However, NanoSIMS can not determine the morphology, elemental composition and mineral species. High-resolution transmission electron microscopy (HRTEM) combined with selected area electron diffraction (SAED) is also a promising

technique that can determine the morphology and provide detailed information on organo-mineral surfaces, as well as changes in their surface chemistries (Wen et al., 2014a; Yaron-Marcovich et al., 2005). Although direct observations of organo-mineral complexes by NanoSIMS and HRTEM have
80 been previously described (Ramos et al., 2013; Vogel et al., 2014; Rumpel et al., 2015), few studies have reported the effects of fertilization practices on the organo-mineral complexes in soil colloids. In addition, X-ray photoelectron spectroscopy (XPS) can identify the oxidation state of elements on the surface (2~10 nm) of minerals (Zhu et al., 2014). Compared with XPS technique, X-ray absorption fine structure spectroscopy (XAFS) is a powerful tool for both identification and quantification of different
85 mineral phases present in soil colloids (Li et al., 2015; Xiao et al., 2015).

Using soil colloids extracted from 24-year fertilized soils (1990-2014), the objective of this study were to address 1) the effects of fertilization practices on the quantity and composition of Al and Fe minerals, and 2) the *in-situ* interactions between SOC and minerals at the submicron scale.

2. Materials and methods

2.1. Soil samples

90

Samples of soil (Ferralic Cambisol, FAO soil taxonomic classification) were from a long-term (1990-2014) fertilization site in Qiyang, Hunan, Southern China (26°45'N, 111°52'E, 120 m above sea level). The long-term fertilization experiment, which belongs to the Institute of Agricultural Resources and Regional Planning, Chinese Academy of Agricultural Sciences, has been under an annual rotation
95 of wheat and corn cropping system since September 1990. The topsoil contained 61.4% clay, 34.9% silt and 3.7% sand. Three fertilization treatments with 2 replicates or plots (20 m × 10 m) for each treatment

were examined as follows: 1) no fertilization (Control), 2) chemical nitrogen (N), phosphorus (P) and potassium (K) (NPK) and 3) a combination of the chemical fertilizers with swine manure (NPKM) (see Fig. S1 for detailed fertilization rates). The NPK and MNPK had the same total application of 300 kg N ha⁻¹ yr⁻¹. The applied N was 100% urea in the NPK, but was 30% from urea with the remaining 70% from swine manure in the MNPK. A 1.0-m-deep cement buffer zone was constructed between each plot. Each soil sample was a composite of twenty random cores (5 cm internal diameter auger) collected at 0-20 cm depth from one replicate plot. The fresh soil was mixed thoroughly, air-dried, and sieved (5 mm) for further analyses.

2.2. Soil colloids extraction and quantitation of highly reactive Al and Fe minerals

The soil colloids extraction was based on a previously described method (Schumacher et al., 2005). Briefly, 100 g of fresh soils was suspended in 500 mL of deionized water on a horizontal shaker (170 rpm) for 8 hr at 25 ± 1°C, and centrifuged at 2500 g for 6 min (Fig. S1). Aliquots of the supernatant suspensions and freeze-dried soil colloid samples were then generated. Quantitation of highly reactive minerals, including Al and Fe minerals (Al_o, Fe_o), was performed using the acid ammonium-oxalate extraction method (Kramer et al., 2012). In brief, soil was extracted using 0.275 M ammonium oxalate at pH 3.25 with a 1:100 soil:extractant (w/v) ratio. Ammonium oxalate was used to selectively remove short-range ordered hydrous oxides of Fe and Al such as ferrihydrite and allophane

2.3. HRTEM analysis

HRTEM samples were prepared by dropping soil mobile colloids onto carbon coated copper grids. The images were recorded at an acceleration voltage of 200 keV using a JEOL JEM-2100F microscope

(JEOL JEM-2100F, Japan), which was at the Analysis and Testing Centre of Nanjing Normal University, China. HRTEM images, selected area electron diffraction (SAED) and energy dispersive X-ray analysis (EDX) were conducted using the JEOL JEM-2100F microscope to characterize soil
120 colloid samples.

2.4. NanoSIMS analyses

For NanoSIMS measurements, several aliquots of the colloidal suspension from these three different fertilization treatments were separately dropped onto a silicon wafer and air-dried. In this study, we chose 6 spots from the NanoSIMS images to show the replicates of each soil colloid sample because
125 the majority of particulate organo-mineral complexes were included and similar according to the characterization of natural colloids (Philippe and Schaumann, 2014; Xiao et al., 2015). For every sample, all 6 spots were analyzed to obtain a reliable data basis for the calculation of the fate of $^{12}\text{C}^-$, $^{27}\text{Al}^{16}\text{O}^-$, and $^{56}\text{Fe}^{16}\text{O}^-$ (Table S2).

The analyses were performed on a NanoSIMS 50L (Cameca, Gennevilliers, France) instrument at
130 the Institute of Geology and Geophysics, Chinese Academy of Sciences, China. Prior to analysis, the gold coating layer (30 nm) and any possible contamination of the sample surface were sputtered using a high primary beam current (pre-sputtering). During the pre-sputtering, the reactive Cs^+ ions were implanted into the sample to enhance the secondary ion yields. The primary beam (~ 0.9 pA) focused at a lateral resolution of 100-200 nm, was scanned over the samples, and the secondary ion images of $^{12}\text{C}^-$,
135 $^{27}\text{Al}^{16}\text{O}^-$, and $^{56}\text{Fe}^{16}\text{O}^-$ were simultaneously collected by electron multipliers with an electronic dead time fixed at 44 ns. The presence of $^{12}\text{C}^-$ ion mass indicated SOC, while the presence of $^{27}\text{Al}^{16}\text{O}^-$ and

$^{56}\text{Fe}^{16}\text{O}^-$ demonstrated Al and Fe minerals, respectively. The estimated depth resolution using 16 keV Cs^+ ions as the primary ion beam was about 15 nm. We compensated for the charging due to the non-conductive mineral particles using the electron flood gun of the NanoSIMS instrument. All measurements were conducted in an imaging mode. The dwell time was 1 ms pixel⁻¹ for all acquisitions. Specific details describing NanoSIMS measurements can be found in previous publications (Vogel et al., 2014; Xiao et al., 2015).

The analyses were carried out on different cluster compositions using Image J software with the OpenMIMS plugin (http://www.nrims.hms.harvard.edu/NRIMS_ImageJ.php). In this study, regions of interest (ROIs) were selected according to the intensity of the secondary $^{12}\text{C}^-$ ion mass. Specifically, the visible SOC surface areas were divided into rich and less rich $^{12}\text{C}^-$ ROIs according to the pixel value extracted from the NanoSIMS images. The $^{12}\text{C}^-$ rich ROIs included the areas above 90 pixels and the $^{12}\text{C}^-$ less rich ROIs included the areas in the range of 90-40 pixels under Control and NPK, while the $^{12}\text{C}^-$ rich ROIs were above 50 pixels and the $^{12}\text{C}^-$ less rich ROIs were in the range of 50-30 pixels under NPKM. The threshold option of the Image J software was used to automatically generate the ROIs from these NanoSIMS images. In doing so, the triangle algorithm was used (Vogel et al., 2014; Xiao et al., 2015). The ROIs of the $^{27}\text{Al}^{16}\text{O}^-$ and $^{56}\text{Fe}^{16}\text{O}^-$ images were combined afterwards to obtain the ROIs according to the distribution of the $^{12}\text{C}^-$ rich ROIs and $^{12}\text{C}^-$ less rich ROIs under different fertilizations conditions (Table S2).

2.5. XPS analyses

The sample preparation for the XPS procedures was adapted from Gerin et al. (2003). The XPS

data were collected using a PHI 5000 Versa Probe X-ray photoelectron spectrometer (UIVAC-PHI, Japan) equipped with a monochromatized Al K α X-ray source (1486.69 eV). The binding energy scale was corrected using the adventitious hydrocarbon C 1s spectrum (C 1s = 284.6 eV) (Zhu et al., 2014).
160 The analyzed zone corresponded to a 300 μm \times 300 μm elliptical spot. The surface charge induced by the photo ejection process was balanced using a flood gun at 6 eV. To optimize the signal to noise ratio, spectra were recorded at a detector resolution corresponding to 0.125 eV per channel. The base pressure in the spectrometer was 6.7×10^{-10} Torr. The XPS data analyses were performed using XPSPEAK 4.1 with Shirley background correction, as referenced at <http://www.lasurface.com/xps/index> and
165 <http://srdata.nist.gov/xps/Default.aspx>. No fixed full width at half maximum (FWHM) values were determined for the spectra of soil colloids collected under contrasting fertilization treatments. Gaussian-Lorentzian ratios were freely fit for all peaks in this study (Liang et al., 2008).

2.6. XAFS spectra analyses

Fe K-edge X-ray absorption fine structure (XANES) and extended X-ray absorption fine structure
170 (EXAFS) spectra were recorded at the beamline 1W1B at the XAFS Station of the Beijing Synchrotron Radiation Facility (BSRF, Beijing, China) using a Si (111) double-crystal monochromator. The storage ring was operated at 2.5 GeV with the electron current decreasing from 240 to 160 mA within approximately 8 hrs. Samples were ground into fine powders and brushed onto tapes, which were then stacked together to yield approximately one X-ray-absorption length at their corresponding metal edges.
175 The intensities of incident and transmitted X-rays were monitored by ionization chambers filled with nitrogen gas. All reported spectra were measured at 20°C. Spectra were collected in quick-scan and

transmission mode. XANES spectra were recorded with 0.5 eV step, counting 10 s from 7,100 to 7,800 eV. EXAFS spectra were recorded up to $k = 14.0 \text{ \AA}^{-1}$, using 1 eV steps and counting for 100–200 s per scan. To improve data quality, 5 XANES scans and 5 EXAFS scans were recorded for each sample. The X-ray energy scale was calibrated to the iron K-edge (7112.0 eV) using an iron metal foil prior to XAFS acquisition. Averaged spectra were normalized using Athena (Version 2.1.1, California, USA) software, and EXAFS data were extracted using the Autoback routine, using the same program. The spectra were normalized by subtracting a first-order polynomial fitted to the data from –100 to –30 eV before the edge and subsequently dividing through a second-order polynomial fitted to the data from 60 to 450 eV above the edge. Linear combination fitting (LCF) of XANES data were performed with the respective functions of Athena. EXAFS spectra were extracted using the Autobk algorithm (Rbkg = 0.9; k-weight = 3, spline k-range 0–11.8 \AA^{-1}). The Fe K-edge XANES spectra with LCF of eight standard iron samples were used to precisely characterize the composition of Fe minerals (Baumgartner et al., 2013; Senn et al., 2015). The standard iron samples of ferrous sulfate, ferrous oxalate, ferric sulfate, ferric oxalate, goethite, hematite, ferrihydrite, and maghemite were also recorded in transmission mode, which were purchased or synthesized (Table S3). A standard was considered to have a substantial contribution if it accounted for more than 10% of a linear combination fit. The quality of the LCF was given by the residual value, the goodness-of-fit parameter R , defined by $R = 6[I_{\text{exp}}(E) - I_{\text{cal}}(E)]^2 / 6[I_{\text{exp}}(E)]^2 \times 100$ where I_{exp} and I_{cal} are the absorption of the experimental and calculated spectra, respectively.

2.7. Chemical analyses

The concentration of SOC was quantified using a CN analyzer (Vario EL, Elementar GmbH, Hanau,

Germany), while SOM was $1.724 \times \text{SOC}$. Soil pH was determined using a pH electrode at a 1:5 soil: distilled water ratio. The concentration of Fe and Al was quantified by inductively coupled plasma atomic emission spectroscopy (710/715 ICP-AES, Agilent, Australia). The concentration of DOC was
200 determined by a TOC/TN analyzer (multi N/C 3000, Analytik Jena AG, Germany).

2.8. Statistical analyses

One-way analysis of variance (ANOVA) was used to test the effects of long-term fertilization on reactive iron minerals in the soil. Significant differences between treatments (means \pm SE, $n = 3$) were determined by Tukey's HSD post hoc test at $P < 0.05$, where the conditions of normality and
205 homogeneity of variance were met.

3. Results

3.1. Concentration and morphology of organo-mineral complexes in soil colloids under contrasting fertilizations

Compared with a soil pH of 5.47 under Control, the soil pH significantly decreased to 4.15 under
210 NPK but significantly increased to 5.84 under NPKM (Table 1). SOM concentrations in different fertilization treatments ranked as NPKM > NPK > Control (Table 1). Oxalate extracted Al (Al_o), Fe (Fe_o), SRO Al (Al_{xps}), Fe (Fe_{xps}), and DOC ranked as NPKM > Control > NPK, but ratios of $\text{DOC}/\text{Al}_{\text{xps}}$ and $\text{DOC}/\text{Fe}_{\text{xps}}$ ranked as NPKM > NPK > Control (Table 1).

To get insight into the spatial distribution of SOM associated with reactive mineral particles, we
215 used both HRTEM and NanoSIMS to acquire *in situ* observations of such associations. At the nanometer scale, the HRTEM images of extracted soil colloids provided direct visualization of the

presence of soil SRO minerals from Control-, NPK- and NPKM-fertilized samples (Fig. 1). Soil minerals showed amorphous and crystalline patterning in different regions (Fig. 1-a, b). The SAED (selected area electron diffraction) pattern further demonstrated that the amorphous mineral species were dominated by Al, Si, and O, while the crystalline minerals were mainly composed of Fe and O (Fig. 1-c, d). The NanoSIMS images of $^{12}\text{C}^-$, $^{27}\text{Al}^{16}\text{O}^-$, and $^{56}\text{Fe}^{16}\text{O}^-$ ion masses showed the submicron elemental distribution and spatial heterogeneity in the soil colloids (Fig. 2). The color bar from blue to white showed that the concentration of $^{12}\text{C}^-$, $^{27}\text{Al}^{16}\text{O}^-$, and $^{56}\text{Fe}^{16}\text{O}^-$ ion masses was from weak to strong on each image.

3.2. Binding capability of C by Al and Fe minerals

We next used the region of interests (ROIs) to explore the C binding capability of Al and Fe minerals. Fig. S2 presents a representative NanoSIMS image showing the position of region of interests (ROIs) among the several replicates (spots) of different fertilization treatments (Control: 8 replicates; NPK: 6 replicates; NPKM: 6 replicates, respectively). Based on the pixel value of secondary $^{12}\text{C}^-$ ion mass in all spots from different fertilization treatments, the selected ROIs were identified. The selected ROIs were further divided into $^{12}\text{C}^-$ rich- and $^{12}\text{C}^-$ less rich- ROIs (Fig. S2). Table S2 lists the quantification of $^{12}\text{C}^-$ rich ($^{12}\text{C}^-$ -R) and $^{12}\text{C}^-$ less-rich ($^{12}\text{C}^-$ -LR) ROIs. The area percentage of the $^{12}\text{C}^-$ rich- or $^{12}\text{C}^-$ less rich- ROIs accounted for 7.47% or 40.18 %, 10.80% or 27.64 % and 8.23% or 37.99% under Control, NPK and NPKM, respectively (Table S2). The area of percentage for the Control and the NPKM was similar but different from the NPK, suggesting that compared to no fertilization, chemical fertilizer can change organo-mineral associations at the submicron scale in soil colloids, but chemical

plus organic fertilization can eliminate the effect of chemical fertilization on organo-mineral associations. Interestingly, the box plots (Fig. 3) of $^{12}\text{C}/^{27}\text{Al}^{16}\text{O}^-$ (a, b) and $^{12}\text{C}/^{56}\text{Fe}^{16}\text{O}^-$ (c, d) ratios showed that both the median and the mean value were higher under NPKM than those under NPK. These results provided *in-situ* observation evidence at the submicron scale demonstrating that more organic C had been bound by Al and Fe minerals under NPKM than under NPK (Figs. 2 and 3), which is consistent with previous results from bulk analysis (Maillard and Angers, 2014)..

3.3. Chemical speciation of reactive minerals and C

The XPS Al 2p_{3/2} peak-fitting results (Table 2 and Fig. 4) showed that 45% allophane (~73.80 eV), 29.4% of boehmite (~74.5 eV) and 26% Al Ox (~75.40 eV) were present in soil colloids under NPKM. In contrast, approximately 43% and 34% of allophane were observed in soil colloids under NPK and Control, respectively. Considering higher (over 5 times) total Al concentrations in soil colloids under NPKM than NPK (Table 1), the amount of allophane in soil colloids under NPKM is approximately 5 times higher than that of NPK.

Linear combination fitting (LCF) of soil colloids (Fig. 5 and Table 3) showed that goethite (56.8%-67.0%) and hematite (14.9%-25.0%) were prominent under all three fertilizations. The remaining Fe phases were composed of the less crystalline ferrihydrite species. The percentage of ferrihydrite was the highest under NPKM ($18.0 \pm 0.02\%$), followed by Control ($16.0 \pm 0.03\%$) and NPK ($6.30 \pm 0.02\%$). In view of the better C binding and potential preservation capability of ferrihydrite when compared to goethite and hematite (Baker et al., 2010; Kramer et al., 2012; Lalonde et al., 2012; Xiao et al., 2015), it is reasonable to conclude that there is greater C loading by Fe minerals under

organic fertilization than under chemical fertilization. This result is consistent with previous meta-analysis (Maillard and Angers, 2014) but provides *in-situ* observation evidence at the submicron scale.

Furthermore, Fe K-edge EXAFS was used for qualitative analysis of the composition of Fe minerals in soil colloids. The Fe k^3 -weighted EXAFS spectra (Fig. 6, left) showed that the spectral features of soils colloids under Control and NPKM were more similar to those of goethite, hematite, and ferrihydrite than to other minerals or compounds, suggesting that those Fe minerals are mainly composed of goethite, hematite, and ferrihydrite. The spectral features of the soils under NPK were more similar to those of goethite and hematite than to those of other minerals or compounds, supporting that those Fe minerals are mainly composed of goethite and hematite rather than short-range ordered ferrihydrite. Specifically, the EXAFS of Fe oxides showed double antinodes at 9.2 and 11.6 \AA^{-1} under Control and NPKM, whereas triple antinodes were observed under NPK at 9.2, 10.3 and 11.6 \AA^{-1} (Fig. 6, left). Double antinodes were found in hematite and ferrihydrite, whereas triple antinodes were observed in goethite. These results implied that the coordination environment for Fe-Fe linkages in Control and NPKM samples might be different from that in NPK samples because the observed peak primarily derived from the Fe-Fe coordination in goethite (Mitsunobu et al., 2012).

Fourier transforms showed that Fe minerals under Control and NPKM had most of the features observed in goethite, hematite, and ferrihydrite [i.e., first peak (Fe-O) and second peak (edge-sharing Fe-Fe)] and amplitude of multiple-scattering peak at 5.2 \AA . Specifically, the first shell at 1.5 \AA corresponds to the Fe-O coordination, and the intensity and position were approximately identical

between the Control or NPKM treated soil colloids and ferrihydrite spectra. In contrast, the second shell identified at $R + \Delta R = 2.3\text{-}3.5 \text{ \AA}$ corresponding to the Fe-Fe coordination was smaller than that of ferrihydrite. These results indicated that Fe in the Control and NPKM treated soil colloids might have a weaker Fe-Fe linkage than that in ferrihydrite.

In addition, the XPS C 1s peak-fitting results (Table 2 and Fig. 4) demonstrated that aromatic C (Ar-C-C/Ar-C-H, $\sim 284.6 \text{ eV}$) was dominant under all three fertilizations, with the highest percentage (75.86%) under NPKM, followed by NPK (62.51%) and Control (62.26%). In contrast, percentages of other carbon groups, i.e., ether or alcohol carbon (C-O) and ketone or aldehyde carbon (C=O), were lowest under NPKM among the three contrasting fertilization treatments.

4. Discussion

4.1. Long-term organic fertilization increased the concentration of highly reactive Al and Fe minerals and their soil C binding capacity

Selective extraction method (Table 1) showed that organic fertilization increased 36.36% of highly reactive Al (Al_0) and 33.33% of highly reactive Fe minerals (Fe_0) compared with Control treatment, but increased 63.64% of Al_0 and 46.67% of Fe_0 compared with NPK treatment. Therefore, organic fertilization facilitates the formation of highly reactive Al and Fe minerals. By ^{27}Al nuclear magnetic resonance (NMR) and Fourier- transform infrared spectroscopy (FTIR) spectroscopy, Wen et al. (2014b) confirmed the presence of amorphous Al as allophane and imogolite in soil colloids under no fertilization and organic fertilization but not under chemical fertilization. However, the direct potential of C preservation capacity by Al and Fe minerals under different fertilizations regimes remains

unexplored. In this study, the ROI analyses of NanoSIMS observation (Fig. 3) provided direct evidence that long-term organic fertilization strengthened the SOC binding and preservation capability of Al and Fe minerals in soil colloids as well as a highly spatial heterogeneity at the submicron scale. Additionally, colloids from the NPKM treated soil had higher ratios of $\text{DOC}/\text{Al}_{\text{xps}}$ and $\text{DOC}/\text{Fe}_{\text{xps}}$ than those under Control and NPK (Table 1), which was compatible with the assumption suggested by the NanoSIMS and HRTEM. These results could be derived from a long-term continuous organic C input that might have enriched soil microbial communities and then in turn supported an efficient formation of the concomitant organo-mineral aggregates (Wild et al., 2014; Basler et al., 2015).

Moreover, it was notable that higher proportion of aromatic C (Ar-C-C/Ar-C-H) while lower proportion of ether or alcohol carbon (C-O) or ketonic or aldehyde carbon (C=O) were observed under NPKM than under NPK or Control, which indicated that additional aromatic functional groups might have a priority attaching to the highly reactive Al and Fe minerals compared with other carbon groups. This result is also supported by C 1s near-edge X-ray fine structure (NEXAFS) spectroscopy that compared to the NPK treatment, the NPKM treatment markedly increased the percentages of both the aromatic (283.0-286.1 eV) and phenolic (286.2-287.5 eV) groups over 2.8-fold (Huang et al., 2016). Moreover, the XPS C 1s peak-fitting results (Table 2 and Fig. 4) demonstrated that the highest percentage of aromatic C (75.86%) was present under NPKM, followed by NPK (62.51%) and Control (62.26%). The previous investigation had shown that aromatic C in composted dairy manure accounted for approximately 30% of the total C, taking advantage of solid-state ^{13}C nuclear magnetic resonance (NMR) spectroscopy (Liang et al., 1996). And the addition of manure-based amendments increased

SOC and enhanced aggregate stability (Mikha et al., 2015). But it is unclear whether manure is direct contributed to aromatic C increase or first utilized by microbes and then contributed to aromatic C increase in this study. Aromatic compounds are preferentially retained at the interface of reactive minerals and that long-term C storage by SRO minerals has occurred via the mechanism of chemical retention with dissolved aromatic acids (Kramer et al., 2012; Huang et al., 2016). These results were due to that the long-term continuous organic C input could improve the spatial arrangement within the mineral matrix (i.e., more amorphous minerals), the fine-scale redox environment (i.e., appropriate pH), microbial ecology (i.e., appropriate pH, manure) and interaction with mineral surfaces under fertile and weakly acidic conditions (Wild et al., 2014; Basler et al., 2015; Lehmann and Kleber, 2015).

4.2. Long-term organic fertilization modified the composition of highly reactive Al and Fe minerals

Our results from both XPS, NanoSIMS and Fe K-edge XAFS showed that organic fertilization facilitated the formation of highly reactive Al and Fe minerals, e.g., allophane, imogolite, and ferrihydrite (Tables 2-3 and Figs. 3-6), which could further explain why long-term organic manure fertilization was able to improve the C and N binding capacity of Al and Fe minerals. The data from the TOC and ICP-AES (Table 1) also supported that soils under NPKM contained significantly higher percentages of Al_o, Fe_o, SRO minerals, and SOM than those under NPK. The results from HRTEM and SAED (Fig. 1) further showed that soil colloids under NPKM were composed of large amounts of meta-stable amorphous or SRO minerals (e.g., allophane, imogolite and ferrihydrite), which could form stable organic-mineral bonds through anion and inner-sphere ligand-exchange reactions and would thus

be well-suited to physically protecting geometries (Torn et al., 1997; Yu et al., 2012; Basler et al., 2015). It would be an innovative method using the ratio of $^{12}\text{C}/^{27}\text{Al}^{16}\text{O}^-$ and $^{12}\text{C}/^{56}\text{Fe}^{16}\text{O}^-$ on NanoSIMS images to quantify the stronger binding ability in NPKM treatment compared with the other treatments (Fig. 3). These results are consistent with previous studies using ^{27}Al NMR spectroscopy and FTIR (Yu et al., 2012; Wen et al., 2014a,b; Wu et al., 2014). Using Fe K-edge XANES spectroscopy, Huang et al. (2016) also showed that reactive Fe minerals were mainly composed of less crystalline ferrihydrite in the M-treated soil and more crystalline goethite in the NPK-treated soil. By measuring the composition of manure, Wen et al. (2014b) had shown that the reactive minerals introduced by the manures were very limited, ruling out the possibility that fertilizers introduced reactive fractions. Furthermore, Huang et al. (2016) indicated that organic fertilization increased the iron freeness index (i.e., Fe_d/Fe_t ratio) when compared to no fertilization and chemical fertilization, suggesting a high degree of soil weathering in organic fertilization. Therefore, we suggest that organic fertilization treatments in situ enhance reactive minerals by the transformation of minerals. This is supported by a simulated study from Huang et al. (2016) that addition of oxalic acid to soil colloids can promote the transformation from Fe(III) to ferrihydrite. Another previous report also indicated that the low-molecular-weight (LMW) organic acid may incorporate into the network structure of SRO minerals, inhibiting further growth of SRO minerals (Xu et al., 2010).

In addition, previous studies have shown that the formation of highly reactive Al and Fe minerals could greatly benefit the binding and potential preservation of SOC (Torn et al., 1997; Wen et al., 2014a; Xiao et al., 2015). Especially, reactive Fe minerals may responsible for the retention of aromatic C and

O-alkyl C in soils (Huang et al., 2016). Under favorable conditions, SOC turnover in soil colloids with highly reactive Al and Fe minerals could persist in tephra beds for at least 250,000 yrs (Parfitt, 2009). Accumulation of highly reactive Al and Fe minerals in soil colloids could therefore improve SOC sequestration under long-term organic manure fertilization. Furthermore, soil colloids usually consist of mixtures or complexes of hydrous oxides of Fe, Al and natural organic matter, which have important implications for deposition, aggregation, and sorption processes (Schumacher et al., 2005; Herrmann et al., 2007; Mueller et al., 2012).

4.3. Environmental implications and technical challenges

Soils are highly complex materials that are structurally and elementally heterogeneous across a wide range of spatial and temporal scales (Herrmann et al., 2007; Mueller et al., 2012; Vogel et al., 2014). In porous media the stability, transport, and deposition of colloids, which usually consist of mixtures or complexes of hydrous oxides of Fe, Al, and natural organic matter, are strongly affected by the mobilized colloidal particles and specific surface area (Kaiser and Guggenberger, 2003; Schumacher et al., 2005). By combining HRTEM, NanoSIMS, XPS and/or XANES technique, the present study investigated the previously unknown highly reactive mineral elements and their spatial distribution patterns under contrasting fertilizations. This strategy has the following key advantages: HRTEM, NanoSIMS images and elemental mapping with sufficient resolution are able to illustrate the specific relationship and spatial heterogeneity of organic, highly reactive mineral complexes under contrasting fertilizations, while decomposition of XPS and Fe K-edge XANES peaks to definite semi-quantitative determinations shows the elemental valence states and compositions. Nevertheless, we are still faced

with the challenge of how to utilize spatial information to parameterize models for handling the complex, stochastic interactions between organo-mineral complexes and their microenvironments, including a range of biogeochemical transformation influenced by different fertilization treatments at the submicron scale (Remusat et al., 2012; Abdala et al., 2015; Hatton et al., 2015). Because of the highly heterogeneous distribution of mineral elements/C-functional groups in soils, investigation on more regions in more samples is necessary to obtain solid relationships between organic C and mineral elements using the NanoSIMS *in situ* observation. Meanwhile, inadequate sample preparation to avoid artefacts is also a challenge, which may introduce a bias in the interpretation of NanoSIMS data and location of regions-of-interest (Herrmann et al., 2007). In addition, the complexity of iron chemistry in soils also makes Fe XANES and EXAFS characterization a challenge. For example, the accuracy of the LCF results is strongly affected by the correctness of the applied set of predictor variables (Prietz et al., 2007). And EXAFS only provides average structural information over a short-range order, therefore it fails to determine if the minerals are crystalline or amorphous (Li et al., 2015), which is important in understanding the stabilization of organic carbon. With the enough soil samples and the improvement of sample preparation, these limitations can be well overcome, and the strategy is expected to receive wide applications in the fields of environmental science.

5. Conclusions

In this study, we showed that long-term (1990-2014) organic fertilization increased the carbon binding loading and the potential preservation capacity of soil colloids at the submicron scale. These submicron scale findings suggest that both reactive mineral species and their associations with C are

differentially affected by inorganic and organic fertilization. This may be attributed to a greater concentration of highly reactive Al and Fe minerals present under NPKM than under NPK. Meanwhile, we also demonstrated that the combination of nano-scale secondary ion mass spectrometry (NanoSIMS),
400 high resolution-transmission electron microscopy (HRTEM), X-ray absorption fine structure spectroscopy (XAFS), and X-ray photoelectron spectroscopy (XPS), is a promising strategy to distinguish relationships between C preservation and minerals in natural soil colloids as well as the potential for SOM accumulation under inorganic and organic fertilizations at the submicron scale. The strategy paves the way toward in situ characterization of organo-mineral associations, which is critical
405 in understanding their associated SOM accumulation and soil carbon storage.

Supplementary material related to this article is available online at:
<http://www.biogeosciences.net/>

Acknowledgment. The authors thank B.R. Wang for his assistance in soil sampling in the Qiyang Long-term Fertilization Station. This work was jointly financially supported by National Natural
410 Science Foundation of China (41371248 and 41371299), Natural Science Foundation of Jiangsu Province of China (BK20131321), the Qing Lan Project, the Innovative Research Team Development Plan of the Ministry of China (IRT1256), the 111 Project (B12009), the Priority Academic Program Development (PAPD) of Jiangsu Higher Education Institutions, and Research Project of Shanghai Municipal Bureau of Quality and Technical Supervision (I00RJ1414).

415 **References**

Abdala, D.B., da Silva, I.R., Vergutz, L., and Sparks, D.L.: Long-term manure application effects on

phosphorus speciation, kinetics and distribution in highly weathered agricultural soils, *Chemosphere*, 119, 504-514, 2015.

420 Baker, L.L., Strawn, D.G., Vaughan, K.L., and McDaniel, P.A.: XAS study of Fe mineralogy in a chronosequence of soil clays formed in basaltic cinders, *Clays Clay Min.*, 58, 772-782, 2010.

Basler, A., Dippold, M., Helfrich, M., and Dyckmans J.: Microbial carbon recycling-an underestimated process controlling soil carbon dynamics-Part 1: A long-term laboratory incubation experiment, *Biogeosciences*, 12, 5929-5940, 2015.

Baumgartner, J., Morin, G., Menguy, N., Perez Gonzalez, T., Widdrat, M., Cosmidis, J., and Faivre, D.:
425 Magnetotactic bacteria form magnetite from a phosphate-rich ferric hydroxide via nanometric ferric (oxyhydr)oxide intermediates, *Proc. Natl. Acad. Sci.*, 110, 14883-14888, 2013. Chen, C.M., Dynes, J.J., Wang, J., Karunakaran, C., Sparks, D.L.: Soft X-ray spectromicroscopy study of mineral-organic matter associations in Pasture soil clay fractions, *Environ. Sci. Technol.*, 48, 6678-6686, 2014.

430 Childs, C.W., Inoue, K., Seyama, H., Soma, M., Theng, B.K.G., and Yuan, G.: X-ray photoelectron spectroscopic characterization of Silica Springs allophane, *Clay Min.*, 32, 565-572, 1997.

Crist, B.V.: Handbook of monochromatic XPS spectra, XPS International, LLC, Mountain View, USA, 2000.

Gerin, P., Genet, M., Herbillon, A., Delvaux, B.: Surface analysis of soil material by X-ray
435 photoelectron spectroscopy, *Eur. J. Soil Sci.*, 54, 589-604, 2003.

Hatton. P.J., Remusat, L., Zeller, B., Derrien, D. A multi-scale approach to determine accurate

elemental and isotopic ratios by nano-scale secondary ion mass spectrometry imaging, *Rap. Commu. Mass Spectro.*, 26, 1363-1371, 2012.

440 Hatton. P.J., Castanha, C., Torn, M.S., and Bird, J.A.: Litter type control on soil C and N stabilization dynamics in a temperate forest, *Glob. Chang. Biol.*, 21, 1358-1367, 2015.

Hernandez, Z., Almendros, G., Carral, P., Alvarez, A., Knicker, H., Perez-Trujillo, J.P.: Influence of non-crystalline minerals in the total amount, resilience and molecular composition of the organic matter in volcanic ash soils (Tenerife Island, Spain), *Eur. J. Soil Sci.*, 63, 603-615, 2012.

445 Hernes, P.J., Kaiser, K., Dyda, R.Y., Cerli, C.: Molecular trickery in soil organic matter: hidden lignin, *Environ. Sci. Technol.*, 47, 9077-9085, 2013.

Herrmann, A.M., Ritz, K., Nunan, N., Clode, P.L., Pett-Ridge, J., Kilburn, M.R., Murphy, D.V., O'Donnell, A.G., Stockdale, E.A.: Nano-scale secondary ion mass spectrometry-A new analytical tool in biogeochemistry and soil ecology: A review article, *Soil Biol. Biochem.*, 39, 1835-1850, 2007.

450 Hochella, M.F.Jr., Lower, S.K., Maurice, P.A., Penn, R.L., Sahai, N., Sparks, D.L., and Twining, B.S.: Nanominerals, mineral nanoparticles, and Earth systems, *Science*, 319, 1631-1635, 2008.

Huang, C.C., Liu, S., Li, R.Z., Sun, F.S., Zhou, Y., and Yu, G.H.: Spectroscopic evidence of the improvement of reactive iron mineral content in red soil by long-term application of swine manure, *PLoS One*, 11, e0146364, 2016.

455 Kaiser, K., and Guggenberger, G.: Mineral surfaces and soil organic matter, *Eur. J. Soil Sci.*, 54, 219-236, 2003.

- Kögel-Knabner, I., Guggenberger, G., Kleber, M., Kandeler, E., Kalbitz, K., Scheu, S., Eusterhues, K., and Leinweber, P.: Organo-mineral associations in temperate soils: Integrating biology, mineralogy, and organic matter chemistry, *J. Plant Nutr. Soil Sci.*, 171, 61-82, 2008.
- 460 Kramer, M.G., Sanderman, J., Chadwick, O.A., Chorover, J., Vitousek, P.M.: Long-term carbon storage through retention of dissolved aromatic acids by reactive particles in soil, *Glob. Chang. Biol.*, 18, 2594-2605, 2012.
- Lalonde, K., Mucci, A., Ouellet, A., Gelinas, Y.: Preservation of organic matter in sediments promoted by iron, *Nature*, 483, 198-200, 2012.
- 465 Lehmann, J., and Kleber M.: The contentious nature of soil organic matter, *Nature*, 528, 60-68, 2015.
- Li, W., Joshi, S.R., Hou, G.J., Burdige, D.J., Sparks, D.L., and Jaisi, D.P.: Characterizing phosphorus speciation of Chesapeake Bay sediments using chemical extraction, ^{31}P NMR, and X-ray absorption fine structure spectroscopy, *Environ. Sci. Technol.*, 49, 203-211, 2015.
- Liang, B., Lehmann, J., Solomon, D., Sohi, S., Thies, J.E., Skjemstad, J.O., Luizao, F.J., Engelhard, 470 M.H., Neves, E.G., and Wirick, S.: Stability of biomass-derived black carbon in soils, *Geochim. Cosmochim. Acta*, 72, 6069-6078, 2008.
- Liang, B.C., Gregorich, E.G., Schnitzer M., and Voroney R.P.: Carbon mineralization in soils of different textures as affected by water-soluble organic carbon extracted from composted dairy manure, *Biol. Fertil. Soils*, 21, 10-16, 1996.
- 475 Maillard, E., and Angers, D. A.: Animal manure application and soil organic carbon stocks: a meta-analysis, *Glob. Chang. Biol.*, 2, 666-679, 2014.

- Mikha, M. M., Hergert, G. W., Benjamin, J. G., Jabro, J. D., and Nielsen, R. A.: Long-term manure impacts on soil aggregates and aggregate-associated carbon and nitrogen, *Soil Sci. Soc. Amer. J.*, 79, 2, 626-636, 2015.
- 480 Mikutta, R., Schaumann, G.E., Gildemeister, D., Bonneville, S., Kramer, M.G., Chorover, J., Chadwick, O.A., and Guggenberger, G.: Biogeochemistry of mineral-organic associations across a long-term mineralogical soil gradient (0.3-4100kyr), Hawaiian Islands, *Geochim. Cosmochim. Acta*, 73, 2034-2060, 2009.
- Mitsunobu, S., Shiraishi, F., Makita, H., Orcutt, B.N., Kikuchi, S., Jorgensen, B.B., Takahashi, Y.:
 485 Bacteriogenic Fe(III) (oxyhydr)oxides characterized by synchrotron microprobe coupled with spatially resolved phylogenetic analysis, *Environ. Sci. Technol.*, 46, 3304-3311, 2012.
- Mueller, C.W., Kölbl, A., Hoeschen, C., Hillion, F., Heister, K., Herrmann, A.M., and Kögel-Knabner, I.: Submicron scale imaging of soil organic matter dynamics using NanoSIMS-From single particles to intact aggregates, *Org. Geochem.*, 42, 1476-1488, 2012.
- 490 Parfitt, R.L.: Allophane and imogolite: role in soil biogeochemical processes, *Clay Min.*, 44, 135-155, 2009.
- Philippe, A. and Schaumann, G.E.: Interactions of dissolved organic matter with natural and engineered inorganic colloids: A review, *Environ. Sci. Technol.*, 48, 8946-8962, 2014.
- Prietz, J., Thieme, J., Eusterhues, K., and Eichert, D.: Iron speciation in soils and soil aggregates by
 495 synchrotron-based X-ray microspectroscopy (XANES, μ -XANES), *Europ. J. Soil Sci.*, 58, 1027-1041, 2007.

- Ramos, M., Ferrer, D., Martinez-Soto, E., Lopez-Lippmann, H., Torres, B., Berhault, G., and Chianelli, R.R.: In-situ HRTEM study of the reactive carbide phase of Co/MoS₂ catalyst, *Ultramicroscopy*, 127, 64-69, 2013.
- 500 Remusat, L., Hatton, P.J., Nico, P.S., Zeller, B., Kleber, M., Derrien, D.: NanoSIMS study of organic matter associated with soil aggregates: advantages, limitations, and combination with STXM, *Environ. Sci. Technol.*, 46, 3943-3949, 2012.
- Rumpel, C., Baumann, K., Remusat, L., Dignac, M.F., Barré, P., Deldicque, D., Glasser, G., Lieberwirth, I., and Chabbi, A.: Nanoscale evidence of contrasted processes for root-derived organic matter stabilization by mineral interactions depending on soil depth, *Soil Biol. Biochem.*, 85, 82-88, 505 2015.
- Schmidt, M.W.I., Torn, M.S., Abiven, S., Dittmar, T., Guggenberger, G., Janssens, I.A., Kleber, M., Kögel-Knabner, I., Lehmann, J., Manning, D.A.C., Nannipieri, P., Rasse, D.P., Weiner, S., Trumbore, S.E.: Persistence of soil organic matter as an ecosystem property, *Nature*, 478, 49-56, 510 2011.
- Schumacher, M., Christl, I., Scheinost, A.C., Jacobsen, C., Kretzschmar, R.: Chemical heterogeneity of organic soil colloids investigated by scanning transmission X-ray microscopy and C-1s NEXAFS microspectroscopy, *Environ. Sci. Technol.*, 39, 9094-9100, 2005.
- Senn, A.C., Kaegi, R., Hug, S.J., Hering, J.G., Mangold, S., and Voegelin, A.: Composition and 515 structure of Fe(III)-precipitates formed by Fe(II) oxidation in water at near-neutral pH: Interdependent effects of phosphate, silicate and Ca, *Geochim. Cosmochim. Acta*, 162, 220-246,

2015.

- Solomon, D., Lehmann, J., Harden, J., Wang, J., Kinyangi, J., Heymann, K., Karunakaran, C., Lu, Y.,
Wirick, S., and Jacobsen, C.: Micro-and nano-environments of carbon sequestration: Multi-element
520 STXM-NEXAFS spectromicroscopy assessment of microbial carbon and mineral associations,
Chem. Geol., 329, 53-73, 2012.
- Torn, M.S., Trumbore, S.E., Chadwick, O.A., Vitousek, P.M., and Hendricks, D.M.: Mineral control of
soil organic carbon storage and turnover, *Nature*, 389, 170-173, 1997.
- Xiao, J., Wen, Y.L., Li, H., Hao, J.L., Shen, Q.R., Ran, W., Mei, X.L., He, X.H., Yu, G.H.: In situ
525 visualisation and characterisation of the capacity of highly reactive minerals to preserve soil organic
matter (SOM) in colloids at submicron scale, *Chemosphere*, 138, 225-232, 2015.
- Vogel, C., Mueller, C.W., Hoschen, C., Buegger, F., Heister, K., Schulz, S., Schlöter, M., and
Kögel-Knabner, I.: Submicron structures provide preferential spots for carbon and nitrogen
sequestration in soils, *Nat. Commun.*, 5, 2947, 2014.
- 530 Wen, Y.L., Li, H., Xiao, J., Wang, C., Shen, Q.R., Ran, W., He, X.H., Zhou, Q.S., and Yu, G.H.:
Insights into complexation of dissolved organic matter and Al(III) and nanominerals formation in
soils under contrasting fertilizations using two-dimensional correlation spectroscopy and high
resolution-transmission electron microscopy techniques, *Chemosphere*, 111, 441-449, 2014a.
- Wen, Y.L., Xiao, J., Li, H., Shen, Q.R., Ran, W., Zhou, Q.S., Yu, G.H., and He, X.H. Long-term
535 fertilization practices alter aluminum fractions and coordinate state in soil colloids, *Soil Sci. Soc.
Am. J.*, 78, 2083-2089, 2014b.

- Wild, B., Schnecker, J., Alves, R.J.E., Barsukov, P., Bárta, J., Čapek, P., Gentsch, N., Gittel, A., Guggenberger, G., Lashchinskiy, N., Mikutta, R., Rusalimova, O., Šantrůčková, H., Shibistova, O., Ulrich, T., Watzka, M., Zrazhevskaya, G., and Richter, A.: Input of easily available organic C and N stimulates microbial decomposition of soil organic matter in arctic permafrost soil, *Soil Biol. Biochem.*, 75, 143-151, 2014.
- Wu, J., Wu, M.J., Li, C.P., Yu, G.H.: Long-term fertilization modifies the structures of soil fulvic acids and their binding capability with Al, *PloS one*, 9, e105567, 2014.
- Xu, R.K., Hu, Y.F., Dynes, J.J., Zhao, A.Z., Blyth, R.I.R., Kozak, L.M., and Huang, P.M.: Coordination nature of aluminum (oxy)hydroxides formed under the influence of low molecular weight organic acids and a soil humic acid studied by X-ray absorption spectroscopy, *Geochim. Cosmochim. Acta*, 74, 6422–6435, 2010.
- Yaron-Marcovich, D., Chen, Y., Nir, S., and Prost, R.: High resolution electron microscopy structural studies of organo-clay nanocomposites, *Environ. Sci. Technol.*, 39, 1231-1238, 2005.
- Yu, G.H., Wu, M.J., Wei, G.R., Luo, Y.H., Ran, W., Wang, B.R., Zhang, J.C., and Shen, Q.R.: Binding of organic ligands with Al(III) in dissolved organic matter from soil: implications for soil organic carbon storage, *Environ. Sci. Technol.*, 46, 6102-6109, 2012.
- Zhao, X., Zhang R., Xue J. F., Pu C., Zhang X.Q., Liu S. L., Chen F., Lal R., and Zhang H. L.: Chapter One-Management-Induced Changes to Soil Organic Carbon in China: A Meta-analysis, *Adv. Agron.*, 134, 1-50, 2015.
- Zhu, T., Lu, X., Liu, H., Li, J., Zhu, X., Lu, J., and Wang, R.: Quantitative X-ray photoelectron

spectroscopy-based depth profiling of bioleached arsenopyrite surface by *Acidithiobacillus ferrooxidans*, *Geochim. Cosmochim. Acta*, 127, 120-139, 2014.

560 **Figure Captions**

Fig. 1. High-resolution transmission electron microscopy (HRTEM) images of highly reactive minerals from colloids extracted from soil (Ferralic Cambisol) from three long-term (1990-2014) fertilization treatments. (a), TEM images; (b), HRTEM images and selected area electron diffraction (SAED) patterns of the two regions indicated by the blue squares, showing that the black region is a complete
565 crystalline, while the grey region is amorphous; (c-d) energy dispersive X-ray analysis (EDX) images of the region 1 and region 2. Control, no fertilization; NPK, chemical nitrogen, phosphorus and potassium fertilization; NPKM, chemical NPK plus swine manure fertilization.

Fig. 2. Representative NanoSIMS images of $^{12}\text{C}^-$, $^{27}\text{Al}^{16}\text{O}^-$ and $^{56}\text{Fe}^{16}\text{O}^-$ in soil colloids from three contrasting long-term (1990-2014) fertilization treatments (Control, no fertilization, $28 \times 28 \mu\text{m}^2$; NPK,
570 chemical nitrogen, phosphorus and potassium fertilization, $30 \times 30 \mu\text{m}^2$; NPKM, chemical NPK plus swine manure fertilization, $25 \times 25 \mu\text{m}^2$). Note that the color intensity calibration bar displayed in the chemical maps corresponds to the relative concentrations of individual elements, but cannot be used to compare one element with another. Bar = $5 \mu\text{m}$.

Fig. 3. Box plots of $^{12}\text{C}^-/^{27}\text{Al}^{16}\text{O}^-$ (a, b) and $^{12}\text{C}^-/^{56}\text{Fe}^{16}\text{O}^-$ (c, d) ratios reflecting the $^{12}\text{C}^-$ rich ROIs (a, c)
575 and $^{12}\text{C}^-$ less rich ROIs (b, d) of the soil colloids from three contrasting long-term (1990-2014) fertilization treatments using NanoSIMS (for all spots). Control, no fertilization; NPK, chemical nitrogen, phosphorus and potassium fertilization; NPKM, chemical NPK plus swine manure fertilization. The $^{12}\text{C}^-$ rich ROIs include the areas above 90 pixels and the $^{12}\text{C}^-$ less rich ROIs include the areas in the range of 90-40 pixels under Control and NPK, which were above 50 pixels and in the range of 50-30

580 pixels under NPKM. The number n in figures represents the number of the selected ROIs. The line in the middle of the box is the median value and the square in the box is the mean value. The lines that protrude out of the boxes represent the 25th and 75th population percentiles. Outliers are shown as diamonds.

Fig. 4. XPS peak-fitting (Al 2p_{3/2}, C 1s) images recorded from soil (Ferralic Cambisol) colloids
585 extracted under three long-term (1990-2014) fertilization treatments. Control, no fertilization; NPK, chemical nitrogen, phosphorus and potassium fertilization; NPKM, chemical NPK plus swine manure fertilization.

Fig. 5. Fe K-edge XANES spectra of reference materials and soil colloids from three contrasting
long-term (1990-2014) fertilization treatments. The scattered circles represent the linear combination
590 fitting (LCF) results of the sample spectra. Control, no fertilization; NPK, chemical nitrogen, phosphorus and potassium fertilization; NPKM, chemical NPK plus swine manure fertilization.

Fig. 6. Fe K-edge EXAFS (left) and Fourier transforms (right) of reference materials and soil colloids
from three contrasting long-term (1990-2014) fertilization treatments. Control, no fertilization; NPK,
chemical nitrogen, phosphorus and potassium fertilization; NPKM, chemical NPK plus swine manure
595 fertilization.

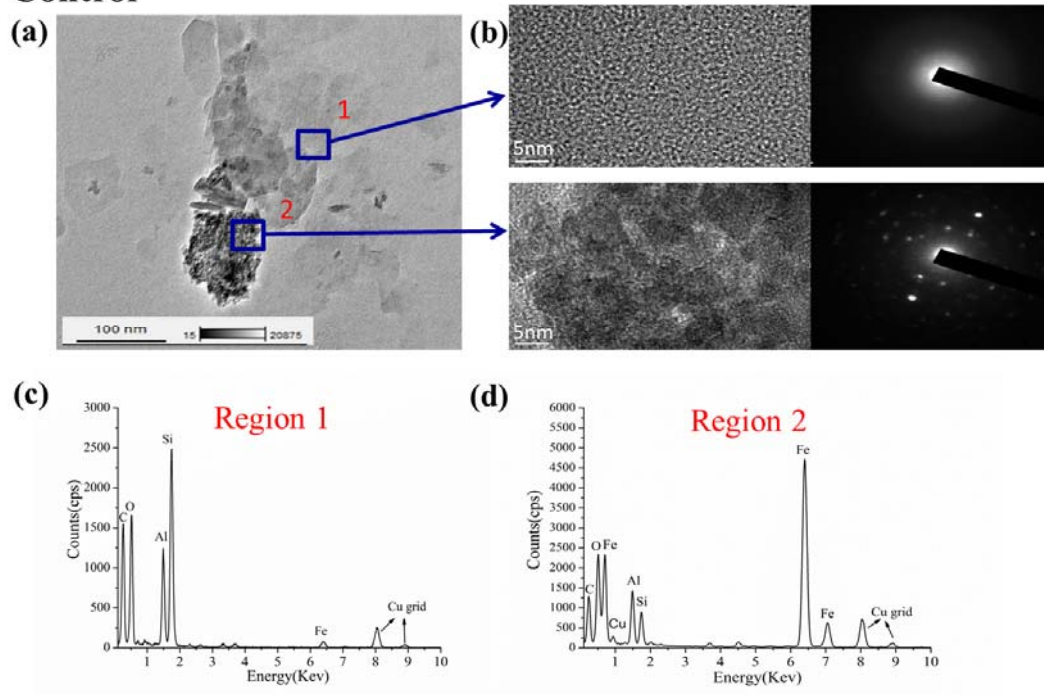
Table Captions

Table 1. Basic physiochemical characteristics of soil samples from three contrasting long-term (1990-2014) fertilization treatments ^a.

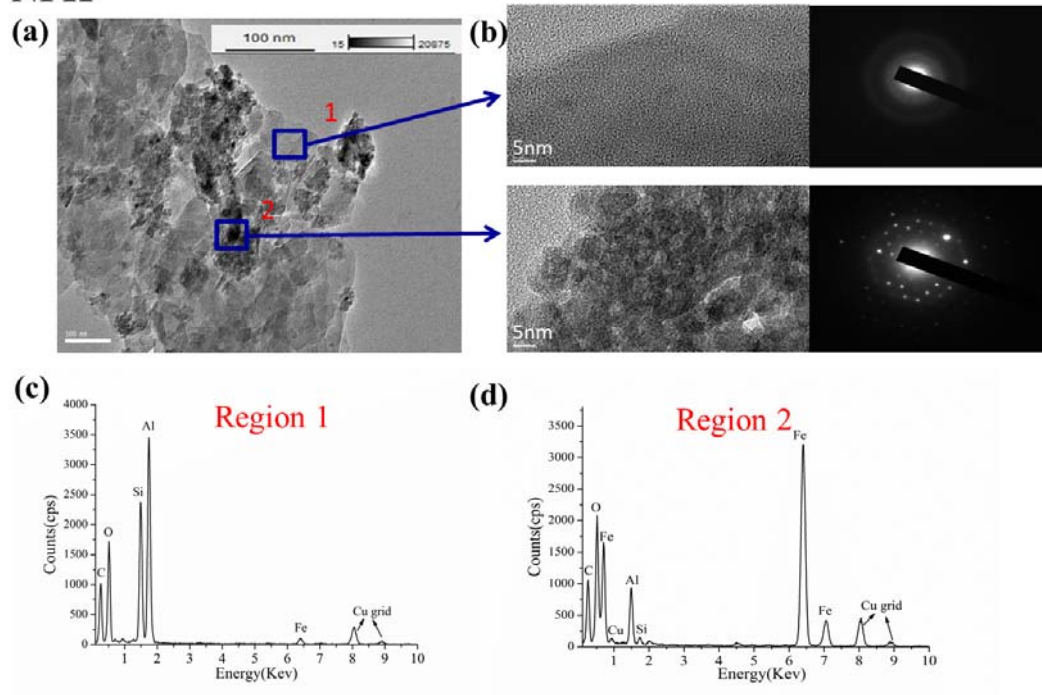
Table 2. Binding energy and quantitation/assignment of XPS spectral bands of soil samples from three
600 contrasting long-term (1990-2014) fertilization treatments ^a.

Table 3. Linear combination fit (LCF) results of Fe K-edge XANES spectra of the soil colloids from three contrasting long-term (1990-2014) fertilization treatments ^a.

Control



NPK



605

NPKM

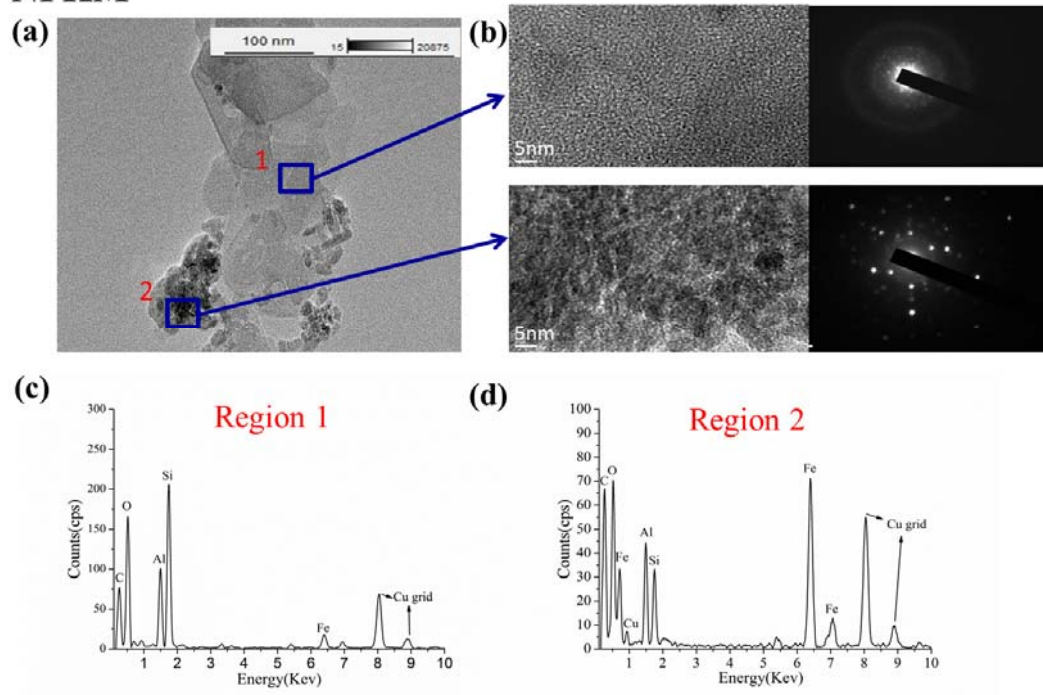


Figure 1

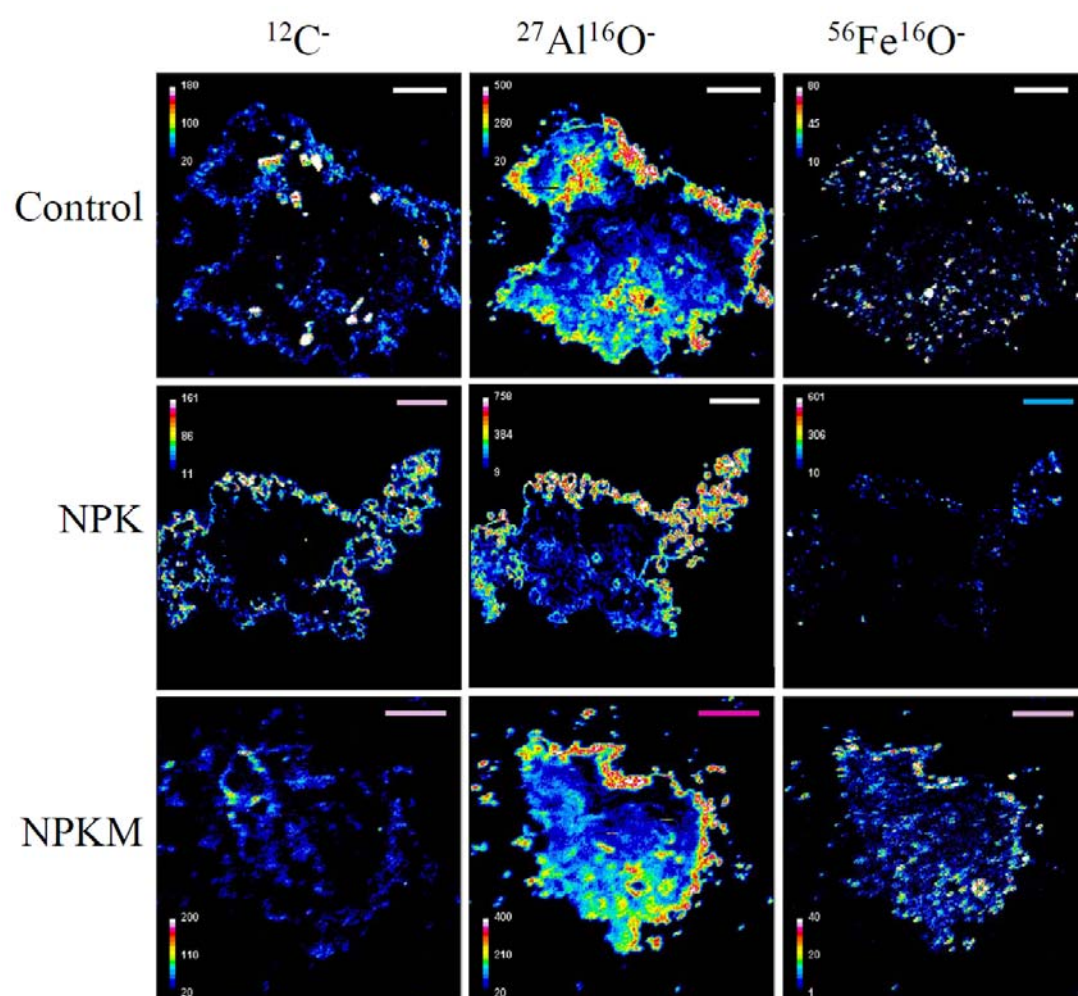


Figure 2

610

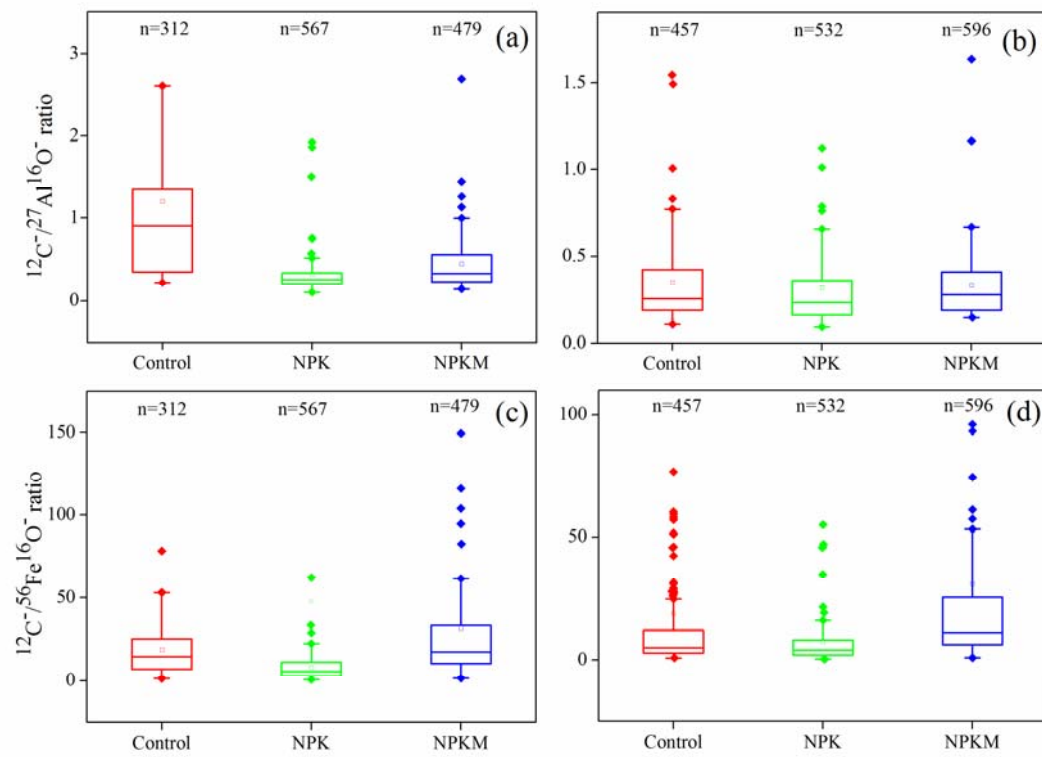
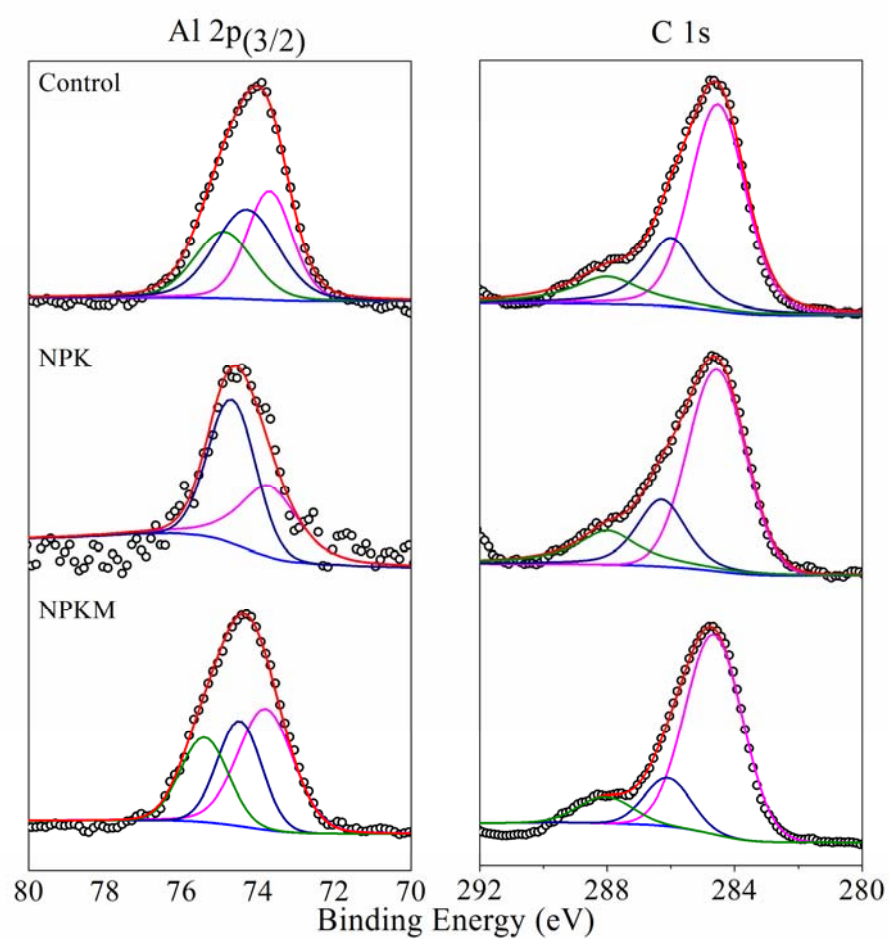


Figure 3



615 **Figure 4**

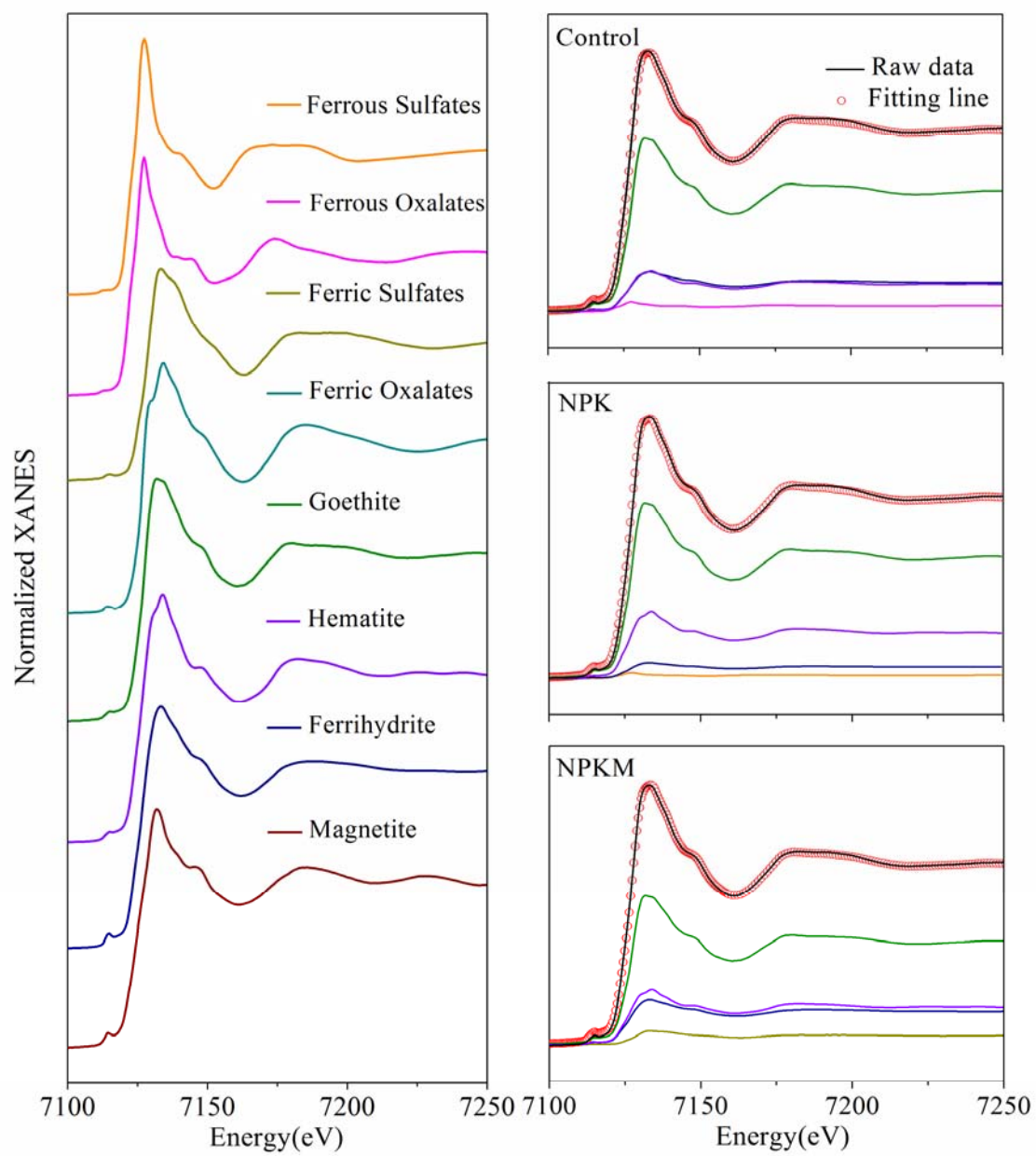
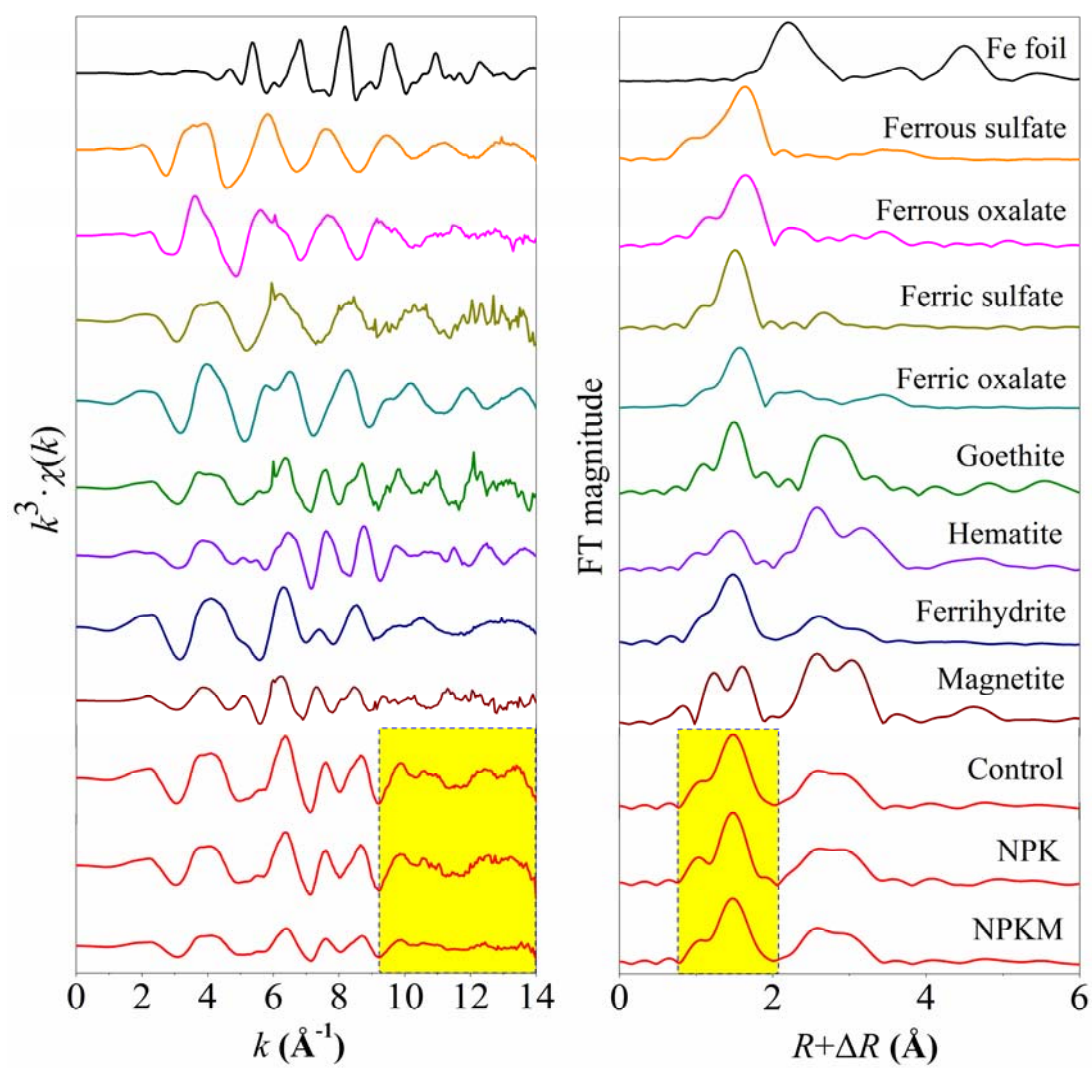


Figure 5



620 **Figure 6**

621 **Table 1. Basic physiochemical characteristics of soil samples from three separate long-term (1990-2014) fertilization treatments ^a.**

Treatmen	Soil					Soil colloids				
t	Bulk soil pH	SOM	Al _o	Fe _o	SRO	Al _{XPS}	Fe _{XPS}	DOC	DOC/Al _{XPS}	DOC/Fe _{XPS}
	(H ₂ O)	(g kg ⁻¹)	(%)	(%)	(%)	(%)	(%)	(mg L ⁻¹)		
Control	5.47 ± 0.04b	14.88 ± 2.02c	0.07 ± 0.003b	0.20 ± 0.004b	0.17 ± 0.00b	6.23	1.47	6.17	0.99	4.20
NPK	4.15 ± 0.00c	18.36 ± 0.16b	0.04 ± 0.003c	0.16 ± 0.003c	0.12 ± 0.00c	1.22	0.48	4.62	3.79	9.63
NPKM	5.84 ± 0.01a	25.13 ± 2.02a	0.11 ± 0.002a	0.30 ± 0.007a	0.26 ± 0.01a	6.84	1.59	42.02	6.14	26.43

622 ^a Note: Control, no fertilization; NPK, chemical nitrogen, phosphorus and potassium fertilization; NPKM, chemical NPK plus swine manure
623 fertilization, SOM, soil organic matter. Al_{XPS} and Fe_{XPS} indicated the surface concentration of Al and Fe in soil colloids, which were determined
624 by the X-ray photoelectron spectroscopy (XPS). Al_o and Fe_o indicated reactive Al and Fe nanominerals, which were extracted using acid
625 ammonium oxalate. DOC, dissolved organic carbon in soil colloids. Short-range ordered (SRO) minerals were calculated using the formula of
626 Al_o + 1/2 Fe_o (%) (Kramer et al., 2012). Significant differences among fertilization treatments were determined using one-way ANOVA followed
627 by the Tukey's HSD post hoc test at *P* < 0.05 after the conditions of normality and homogeneity of variance were met.

628

629 **Table 2. Binding energy and quantitation/assignment of XPS spectral bands of soil samples from three separate long-term (1990-2014)**
630 **fertilization treatments ^a.**

Element	Control			NPK			NPKM		
	Peak (eV)	Atomic (%)	Assignment	Peak (eV)	Atomic (%)	Assignment	Peak (eV)	Atomic (%)	Assignment
Al 2p_{3/2}	73.8	34.2	Allophane Al ₂ O ₃ / Al ₂ O ₃ -nH ₂ O	73.8	42.9	Allophane Al ₂ O ₃ / Al ₂ O ₃ -nH ₂ O	73.8	45.1	Allophane Al ₂ O ₃ / Al ₂ O ₃ -nH ₂ O
Al 2p_{3/2}	74.3	39.0	Boehmite AlO(OH)	74.7	57.1	Boehmite AlO(OH)	74.5	29.4	Boehmite AlO(OH)
Al 2p_{3/2}	74.9	26.8	AlOx	/	/	/	75.4	25.5	AlOx
C 1s	284.6	62.3	Aromatic carbon (Ar-C-C/Ar-C-H)	284.6	62.5	aromatic carbon (Ar-C-C/Ar-C-H)	284.6	75.9	aromatic carbon (Ar-C-C/Ar-C-H)
C 1s	286.1	23.6	Ether or alcohol carbon (C-O)	286.2	20.8	Ether or alcohol carbon (C-O)	286.1	14.7	Ether or alcohol carbon (C-O)
C 1s	288.0	14.2	Ketonic or aldehyde carbon (C=O)	288.0	16.7	Ketonic or aldehyde carbon (C=O)	288.0	9.5	Ketonic or aldehyde carbon (C=O)

631 ^a Note: Control, no fertilization; NPK, chemical nitrogen, phosphorus and potassium fertilization; NPKM, chemical NPK plus swine manure
632 fertilization. The atomic percentage (%) is the corrected value calculated from the XPS peak-fitting areas (Childs et al., 1997; Crist, 2000) and
633 elemental assignments were determined from published studies (Liang et al., 2008; Mikutta et al., 2009; Xiao et al., 2015).

634

635 **Table 3. Linear combination fit (LCF) results of Fe K-edge XANES spectra of the soil colloids from three separate long-term (1990-2014)**
636 **fertilization treatments ^a.**

Treatment	LCF results (%)						LCF parameters	
	Goethite	Hematite	Ferrihydrite	Ferric sulfates	Ferrous citrates	Ferrous sulfates	R-factor	Chi-square
Control	66.0 ± 0.025	14.9 ± 0.000	16.0 ± 0.025	ND	3.10 ± 0.012	ND	0.000052	0.00437
NPK	67.0 ± 0.025	25.0 ± 0.000	6.30 ± 0.020	ND	ND	1.70 ± 0.008	0.000051	0.00426
NPKM	56.8 ± 0.025	20.4 ± 0.000	18.0 ± 0.017	4.8 ± 0.018	ND	ND	0.000051	0.00436

637 ^a Note: Control, no fertilization; NPK, chemical nitrogen, phosphorus and potassium fertilization; NPKM, chemical NPK plus swine manure
638 fertilization. ND, not detected. Determination of parameters of fit (i.e., R-factor and chi-square) indicated that the LCF results are convincing.